 CMC, vol.17, no.2, pp.127-147, 2010

Deformation and Failure of Single-Packets in Martensitic Steels

T.M. Hatem[1] **and M.A. Zikry**[1]

Abstract: A three-dimensional multiple-slip dislocation-density-based crystalline formulation, and specialized finite-element formulations were used to investigate dislocation-density evolution and crack behavior in single-packet lath martensite in high strength martensitic steels. The formulation is based on accounting for variant morphologies and orientations, and initial dislocations-densities that are uniquely inherent to martensitic microstructures. The effects of loading plane with respect to the orientation o the habit plane are investigated. Furthermore, the formulation was used to investigate single-packet microstructure mapped directly from SEM/EBSD images of maraging and ausformed martensitic steel alloys. This analysis underscores that shear pipe effects in martensitic steels, where the long direction of the laths is aligned with specific slip-directions, can result in shear-strain localization along specific variants. Furthermore, the results indicate that the strength and ductility are higher for the loading plane parallel to the habit plane as compared to those normal to the habit plane.

Keywords: lath martensite, dislocation-density, high strength steel, shear-strain localization.

1 Introduction

Lath martensite microstructures have distinct orientations, distributions, and morphologies pertaining to martensitic transformations, and these characteristics have interrelated effects on inelastic deformation and failure in high strength steels, see, for example, (Krauss (2003), Wasaka and Wayman (1981), Sandvik and Wayman (1983), Morito *et al.* (2003, 2005, 2006), and Rowenhorst *et al.* (2006). Specifically, the interrelated effects of lath martensite (b.c.c.) morphology, parent austenite (f.c.c.) orientation, strains related to transformations from f.c.c. to b.c.c. structures, and retained austenite can affect deformation and failure in martensitic steels.

[1] Department of Mechanical and Aerospace Engineering, North Carolina State University, Raleigh, North Carolina 27695-7910, USA.

Due to the fine microstructure of lath martensite, it has been difficult to fully characterize lath martensite and understand its effect on overall behavior. Wayman (see, for example, Wasaka and Wayman (1981) and Sandvik and Wayman (1983)) conducted a series of pioneering experiments that identified lath martensite's characteristics, such as the habit plane of lath martensite and martensite Orientation Relations (ORs); the lath microstructure in successive layers; the internal and interfacial dislocation microstructure in lath martensite. Kelly (1992) utilized Wayman's work to interpret lath martensite microstructure using phenomenological theory to elucidate how martensitic diffusionless transformation occurs. In recent years, Morito and his colleagues (2003, 2006, 2006) have conducted significant experiments, utilizing TEM, SEM and EBSD characterization to classify how martensitic structures can be characterized in categories of laths, blocks (variants with low angle orientation relations) and packets (collection of blocks with the same habit plane) microstructures and to characterize their orientation relations and distributions. Rowenhorst *et al.* (2006) have used EBSD and serial sectioning to construct a 3D morphology of coarse martensite lath.

While the martensitic blocks and packets are considered as the origin of the mechanical behavior of martensitic steels (see, for example, Krauss (2003) and Morito *et al.* (2006a)), very few experimental and numerical studies have been focused on investigating deformation and failure in a single-packet microstructure of lath martensitic steel (c.f. Shtremel, Andreev and Kozlov (1999)).

Most computational investigations pertaining to martensitic steels utilize phenomenological plasticity models, see, for example, McVeigh *et al.* (2007), Zhai and Tomar (2004), and Bandstra *et al.* (2006). These approaches do not account for the crystalline structure and the inherent anisotropy of martensite. Furthermore, critical martensitic characteristics, such as ORs, morphologies, parent austenite orientations, initial dislocation-densities, and retained austenite are not accounted for in these studies. Molecular dynamic (MD) simulations have been invaluable for predicting defect nucleation and transformation at the molecular level, see, for example, Grujicic and Dang (1995), Suzuki (2006), and Marian *et al.* (2003). However, there are severe limitations related to temporal and spatial scales that minimize understanding or predicting behavior at the relevant microstructural level.

To address these limitations and to obtain greater predictive capabilities, we have extended the dislocation-density based crystalline models proposed by Zikry and Kao (1996) and Ashmawi and Zikry (2000) to b.c.c. crystalline microstructures, see Hatem and Zikry (2009a) to investigate deformation and failure in a single packet microstructure of lath martensitic steels. Within this formulation, we account for martensitic transformations and parent austenite crystalline orientations for an accurate OR description of lath microstructure. This representation is based on arranging variants within the blocks that are categorized in terms of habit planes and orientations. These are coupled with specialized finite-element formulations for a predictive framework related to martensitic steels. The formulation is used to investigate how deformation and failure behavior can be affected by the loading plane and its orientation with respect to the habit plane in a single packet lath martensitic steel.

This paper is organized as follows: the dislocation-density crystalline plasticity formulation is given in Section 2, the martensitic microstructure representation in terms of orientation, morphology, retained austenite and initial dislocation-density is outlined in Section 3, the computational techniques are given in Section 4, the results are given in Section 5, and a summary of the results is discussed in Section 6.

2 Dislocation-Density Based Multiple-Slip Constitutive Formulation

The formulation for the multiple-slip crystal plasticity rate-dependent constitutive relations, and the derivation of the evolutionary equations for the mobile and immobile dislocation-densities, which are coupled to the multiple-slip crystalline formulation, are outlined here. A detailed formulation is given by Zikry and Kao (1996) and Ashmawi and Zikry (2000).

It is assumed that the velocity gradient can be decomposed into a symmetric part, the deformation rate tensor, D_{ij} and an anti-symmetric part, the spin tensor, W_{ij}. It is further assumed that the total deformation rate tensor, and the total spin tensor, D_{ij} can be then additively decomposed into elastic and plastic components as

$$D_{ij} = D_{ij}^{*} + D_{ij}^{P}, \quad W_{ij} = W_{ij}^{*} + W_{ij}^{P} \tag{1}$$

in which W_{ij} includes the rigid body spin. The inelastic parts are defined in terms of the crystallographic slip rates as

$$D_{ij}^{P} = P_{ij}^{(\alpha)} * \dot{\gamma}^{(\alpha)}, \quad W_{ij}^{P} = \omega_{ij}^{(\alpha)} * \dot{\gamma}^{(\alpha)}, \tag{2}$$

where α is summed over all slip - systems, and and are second order tensors, and are defined in terms of the unit normals to the slip planes and the unit slip vectors to the slip directions.

For rate - dependent inelastic materials, the constitutive description on each slip - system can be characterized by a power law relation as

$$\dot{\gamma}^{(\alpha)} = \dot{\gamma}_{ref}^{(\alpha)} \left[\frac{\tau^{(\alpha)}}{\tau_{ref}^{(\alpha)}} \right] \left[\frac{\left|\tau^{(\alpha)}\right|}{\tau_{ref}^{(\alpha)}} \right]^{1/m-1} \quad \text{no sum on } \alpha, \tag{3}$$

where $\dot{\gamma}^{(\alpha)}$ is the reference shear strain rate which corresponds to a reference shear stress, $\tau_{ref}^{(\alpha)}$ and m is the rate sensitivity parameter. The reference stress that is used here is a modification of widely used classical forms Mughrabi (1987) that relate the reference stress to a square root dependence on the dislocation - density as

$$\tau_{ref}^{(\alpha)} = \tau_y^{(\alpha)} + Gb \sum_{\xi=1}^{12} a_\xi \sqrt{\rho_{im}^{(\xi)}}, \tag{4}$$

where G is the shear modulus, b is the magnitude of the Burgers vector, $\tau_y^{(\alpha)}$ is the static yield stress, and the coefficients, a_ξ are interaction coefficients, and generally have a magnitude of unity, which imply equal interaction between all slip - systems. This simplification was necessary relative to more involved problem of b.c.c. crystal structure in steel martensite.

2.1 The Evolution of Mobile and Immobile Dislocation-Densities

It is assumed that at a given state for a deformed material, the dislocation structure of total dislocation-density, $\rho^{(\alpha)}$, can be assumed to be additively decomposed, into a mobile dislocation - density, $\rho_m^{(\alpha)}$, and an immobile dislocation - density $\rho_{im}^{(\alpha)}$ as

$$\rho^{(\alpha)} = \rho_m^{(\alpha)} + \rho_{im}^{(\alpha)} \tag{5}$$

It is assumed that during an increment of strain, an immobile dislocation - density rate is generated and an immobile dislocation - density rate is annihilated for statistically stored dislocation - densities (see for example, Liu et al. (1998)). The balance between dislocation generation and annihilation equations is the basis for the evolution of mobile and immobile dislocation - densities as a function of strain. Based on these arguments, it can be shown for a detailed presentation, see Kameda and Zikry (1996), that the coupled set of nonlinear evolutionary equations of mobile and immobile dislocation - densities can then be given by

$$\frac{d\rho_m^{(\alpha)}}{dt} = \dot{\gamma}^{(\alpha)} \left(\frac{g_{sour}}{b^2} \left(\frac{\rho_{im}^{(\alpha)}}{\rho_m^{(\alpha)}} \right) - \frac{g_{minter}}{b^2} \exp\left(-\frac{H}{kT} \right) - \frac{g_{immob}}{b} \sqrt{\rho_{im}^{(\alpha)}} \right), \tag{6}$$

$$\frac{d\rho_{im}^{(\alpha)}}{dt} = \dot{\gamma}^{(\alpha)} \left(\frac{g_{minter}}{b^2} \exp\left(-\frac{H}{kT} \right) + \frac{g_{immob}}{b} \sqrt{\rho_{im}^{(\alpha)}} - g_{recov} \exp\left(-\frac{H}{kT} \right) \rho_{im}^{(\alpha)} \right), \tag{7}$$

where g_{sour} is a coefficient pertaining to an increase in the mobile dislocation - density due to dislocation sources, g_{minter} is a coefficient related to the trapping of mobile dislocations due to forest intersections, cross - slip around obstacles, or dislocation interactions, g_{recov} is a coefficient related to the rearrangement and annihilation of immobile dislocations, g_{immob} is a coefficient related to the immobilization of mobile dislocations, H is the activation enthalpy, and k is Boltzmann's constant. As these evolutionary equations indicate, the dislocation activities related to recovery and trapping are coupled to thermal activation.

The evolutionary equations are coupled to the multiple - slip crystal plasticity formulation, the four g coefficients in eqs. (6 - 7), and the enthalpy, H, must be determined as functions of the deformation mode. The enthalpy, H, is determined by defining an exponential ratio of the current temperature to the reference temperature. The four g coefficients are determined by using the following two general conditions, pertinent to the evolution of dislocation - densities in crystalline materials that the mobile and immobile densities saturate at large strains, and that the relaxation of the mobile dislocation - density to a quasi - steady state value occurs much faster than the variation of the immobile density, see, for example, Mughrabi (1987), Bay et al. (1992), and Hansen (1990).

3 Martensitic Microstructural Representation

The martensitic microstructure has to be accurately represented in terms of orientation, morphology, secondary-phases structures, and transformation dislocation-densities. As experimentally noted by several investigators Krauss (2003) and Morito *et al.* (2006a), these dominant interrelated four characteristics are needed to account for the martensitic microstructure, since they collectively have a significant interrelated role in understanding and predicting behavior at different physical scales. The representation of each of these characteristics is outlined in the following subsections.

The martensitic phase will be represented as (b.c.t./b.c.c.) with twenty four potential slip-systems with $\{110\}$ and $\{112\}$ slip-planes of for easy and pencil glide, and slip directions of <111>, see, for example, Franciosi (1983), and Stainier *et al.* (2002).

3.1 Martensitic Orientations

For the crystalline plasticity formulation, the product phase martensite must be related to the global coordinates through a parent austenite grain orientation and variant orientations. Commonly accepted ORs for lath martensitic steels are Kurdjumov-Sachs (K-S) and Nishiyama-Wassermann (N-W) ORs as given by Bhadeshia (2001).

K-S ORs are based on a γ austenite transformation to an α' martensitic transformation as $(111)_\gamma//(011)_{\alpha'}$, $[\bar{1}01]_\gamma//[\bar{1}\bar{1}1]_{\alpha'}$. For an N-W OR, the transformation is based on $(111)_\gamma//(011)_{\alpha'}$, $[\bar{1}\bar{1}2]_\gamma//[0\bar{1}1]_{\alpha'}$ relation, which is a K-S OR with a 5.12° degree rotation around the $[011]_\gamma$ direction. Investigations by Wasaka and Wayman (1981), Sandvik and Wayman (1983), Morito *et al.* (2003a, 2006b) have clearly indicated that martensitic steel alloys generally have intermediate ORs that are between K-S and N-W ORs. Twenty-four variants can be obtained for K-S ORs. Tab 1 shows the six variants corresponding to the habit plane of $(111)_\gamma$.

Table 1: The six variants corresponding to K-S OR and habit plane $(111)_\gamma$.

Variant No.	Parallel Planes	Parallel Directions
1	$(111)_\gamma$ // $(011)_{\alpha'}$	$[\bar{1}01]_\gamma$ // $[\bar{1}\bar{1}1]_{\alpha'}$
2		$[\bar{1}01]_\gamma$ // $[\bar{1}1\bar{1}]_{\alpha'}$
3		$[0\bar{1}1]_\gamma$ // $[\bar{1}\bar{1}1]_{\alpha'}$
4		$[0\bar{1}1]_\gamma$ // $[\bar{1}1\bar{1}]_{\alpha'}$
5		$[1\bar{1}0]_\gamma$ // $[\bar{1}\bar{1}1]_{\alpha'}$
6		$[1\bar{1}0]_\gamma$ // $[\bar{1}1\bar{1}]_{\alpha'}$

A martensitic transformation is a military transformation where atoms have a fixed relation to each other during the transformation. Martensitic transformations are diffusionless, as it usually occurs at high speed and/or low temperatures, which mandate glissile interfaces between parent and product phases. This interface is the habit plane. The orientation of the habit planes is critical in determining the appropriate martensitic orientations relative to the parent austenite phase. Sandvik and Wayman (1983), Kelly (1992) and Morito *et al.* (2003a, 2006b) have identified $(557)_\gamma$ plane as lath martensite's habit plane.

As noted earlier an essential aspect of representing martensitic texture is to relate the martensitic b.c.c. local grain orientation to the global orientation. Three transformations are needed. The first transformation, $[\mathrm{T}]_1$, relates an observed OR to a theoretical OR, such as K-S and N-W ORs. The second transformation, $[\mathrm{T}]_2$, relates a martensite OR to the parent austenite grain orientation. The third transformation, $[\mathrm{T}]_3$, relates the austenite grain orientation to the global coordinates. These transformations are given by

$$[X]_{Global} = [T]_3 * [T]_2 * [T]_1 * [X]_{\alpha'} \tag{8}$$

Variants are usually deviated from theoretical ORs with random or fixed angles. The first transformation transforms observed martensitic coordinates to a martensitic orientation, such as KS or NW, as

$$[X]_{th\alpha'} = [T]_1 * [X]_{Ob\alpha'} \tag{9}$$

For example, observed orientations for lath martensite, can be represented as a misorientation from $[011]_\gamma$ in K-S OR with an angle ϕ, see, for example, Morito *et al.* (2003a, 2006b), and can be represented as

$$\begin{bmatrix} t/2+c & -s/\sqrt{2} & t/2 \\ s/\sqrt{2} & c & -s/\sqrt{2} \\ t/2 & s/\sqrt{2} & t/2+c \end{bmatrix}, \tag{10}$$

where $s = \sin(\phi)$, $c = \cos(\phi)$, and $t = 1 - \cos(\phi$, and ϕ generally varies between $0°$ and $5.12°$ degree for lath martensitic steels.

The second transformation is the theoretical transformation between the product martensitic phase and the parent austenitic phases, such as the KS OR. The second order tensor for the transformation is obtained utilizing the OR for the invariant plane and axis for each variant. A matrix with an orthogonal parallel system of axes can be used for both parent and product phases since $[X]_\gamma = [T]_2 * [X]_\alpha$ and therefore $[T]_2 = [X]_{\alpha'}^{-1} * [X]_\gamma$. For the first variant in Tab. 1, we would have

$$[X]_\gamma = \begin{bmatrix} 1/\sqrt{3} & -1/\sqrt{2} & 1/\sqrt{3} \\ 1/\sqrt{3} & 0 & -2/\sqrt{6} \\ 1/\sqrt{3} & 1/\sqrt{2} & 1/\sqrt{2} \end{bmatrix},$$

and

$$[X]_{\alpha'} = \begin{bmatrix} 0 & -1/\sqrt{3} & 2/\sqrt{6} \\ 1/\sqrt{2} & -1/\sqrt{3} & -1/\sqrt{6} \\ 1/\sqrt{2} & 1/\sqrt{3} & 1/\sqrt{2} \end{bmatrix}, \tag{11}$$

and,

$$[T]_2 = \begin{bmatrix} 0.7416 & 0.6498 & 0.1667 \\ -0.6667 & 0.7416 & 0.0749 \\ -0.0749 & -0.1667 & 0.9832 \end{bmatrix} \tag{12}$$

Similar transformations can be obtained for all 24 variants related to K-S ORs as presented in part in Tab. 1.

The third transformation pertains to the austenite orientation relative to the global axis and the loading directions. Such a transformation is usually represented as three independent Euler angles, where $[T]_3$ can be obtained. Another approach is similar to the approach utilized to obtain $[T]_2$; $[X]_G = [T]_3 * [X]_\gamma$, and $[T]_3 = [X]_\gamma^{-1} * [X]_G$. For example, to align the load with $(111)_\gamma$ and $[-110]_\gamma$, where $[010]_G//[111]_\gamma$,

$[001]_G$// $[-110]_\gamma$, and $[-110]_\gamma$x $[111]_\gamma$ // $[100]_G$, the transformation would be

$$[X]_\gamma = \begin{bmatrix} 1/\sqrt{6} & 1/\sqrt{3} & -1/\sqrt{2} \\ -1/\sqrt{6} & 1/\sqrt{3} & 1/\sqrt{2} \\ -2/\sqrt{6} & 1/\sqrt{3} & 0 \end{bmatrix},$$

and

$$[X]_G = \begin{bmatrix} 1 & 0 & 0 \\ 0 & 1 & 0 \\ 0 & 0 & 1 \end{bmatrix}, \tag{13}$$

then

$$[T]_3 = \begin{bmatrix} -0.4083 & -0.4083 & 0.8165 \\ 0.5774 & 0.5774 & 0.5774 \\ -0.7071 & 0.7071 & 0.0 \end{bmatrix}, \tag{14}$$

and the final transformation to the global axis can be calculated as in eq. 8.

3.2 Morphology: Variant Arrangement and Distribution

Another unique characteristic of martensitic microstructure is the fine structure of laths, which are the building cells of the martensitic microstructure. The lath long direction is oriented along the $[011]_\gamma$ direction, as illustrated in Fig. 1. A typical lath geometry is on the order of 0.3 x 2.8 x 100 μm (Wasaka and Wayman (1981b)). The change in lath width is small relative to the change in the parent austenite grain, Morito *et al.* (2005).

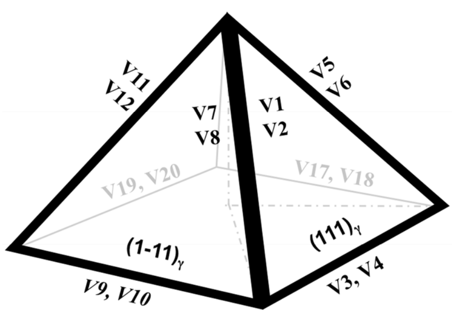

Figure 1: Variant alignments, three main relations can be identified: flat, sharp, and extended inward.

To characterize the complex martensitic microstructure that occurs on different length scales, we will follow what Morito *et al.* (2003, 2005, 2006) have proposed based on SEM and EBSD characterization. Specifically, we will designate a block as a group of laths with low angle misorientations, and a packet as a collection of blocks with the same habit plane (Fig. 2). Using this methodology, we can use the ORs and original austenite orientations to model different variant orientations for different blocks. Due to the microstructural scale that we use in this investigation, the martensitic block is assumed as the smallest scale. Furthermore, as noted by Morito *et al.* (2006a) martensitic properties are more likely to be related to block size interfacial orientations. In this study, a single martensitic packet models will be considered to further elucidate how loading plane, blocks' orientation and size, initial dislocation-densities affect deformation and fracture properties.

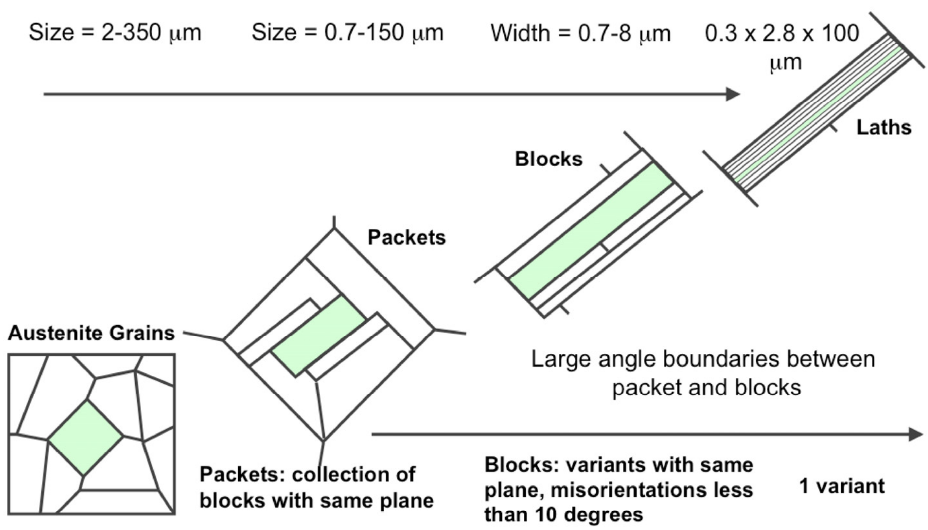

Figure 2: Lath martensite hierarchical microstructure for four scale architecture; parent austenite grains, packets, blocks, and laths.

3.3 Secondary-Phase Structures

Secondary-phases microstructures are frequently observed in high strength steels, such as inclusions and retained austenite. Results for retained austenite and inclusions and their effects are presented by Hatem and Zikry (2009a).

3.4 Transformation Dislocations-Densities

Martensitic transformations are usually associated with high dislocation-densities, see, for example, Sandvik and Wayman (1983), and Morito *et al.* (2003c). These high dislocation-densities are necessary to accommodate the phase transformation and the subsequent glissile interface. Sandvik and Wayman (1983) classified the dislocations in martensitic microstructure as two basic types, transformation and interface dislocations. The transformation dislocations are screw dislocation in all four $<111>_{\alpha'}$ direction, with a/2 $[\overline{1}\overline{1}1]_{\alpha'}$ as the dominant direction. Morito *et al.* (2003c) conducted several experimental studies to characterize the dislocation-densities in nickel and carbon based steels with varying composition. Approximate dislocation-densities of the value of 3.8×10^{14} m^{-2} were obtained for low-nickel lath martensitic steels (Fe-11Ni), Morito *et al.* (2003c).

The percentages of mobile to immobile dislocation-densities ratio were not obtained by these studies, as it is difficult to obtain these values experimentally. The initial mobile and immobile dislocations incorporated in the current study were obtained from numerical models based on a proposed transformation crystalline plasticity model, Hatem and Zikry (2009b).

4 Computational Techniques

The total deformation rate tensor, D_{ij}, and the plastic deformation rate tensor, D^P_{ij} are needed to update the material stress state. The method used here is the one developed by Zikry (1994) for rate-dependent dynamic crystalline plasticity formulations, and only a brief outline will be presented here. An explicit central difference finite element method is used to obtain the total deformation rate tensor, D_{ij}. To overcome numerical instabilities associated with stiffness, a hybrid explicit-implicit method is used to obtain the plastic deformation rate tensor, D^P_{ij}. This hybrid numerical scheme is also used to update the evolutionary equations for the mobile and immobile densities.

5 Results and Discussion

The multiple-slip dislocation-density based crystal plasticity formulation, and the specialized finite element algorithm were used to investigate the shear-strain localization and failure behavior of a single-packet of martensitic steel. The martensite orientation and morphology are represented as outlined in section 3. To investigate the anisotropic behavior of lath martensitic steels with respect to the loading and habit planes, we investigated two loading planes (see Fig. 3). In Model 1, we assume a loading plane for the habit plane $(111)_\gamma$. For Model 2, we assume a loading plane of $(11\overline{2})_\gamma$ normal to the first habit plane. The loading direction for both planes is assumed to be in the direction of $[10]_\gamma$. The K-S relation is used for the martensite OR. Aggregate size can vary significantly for different loading planes (see, for example, Shtremel, Andreev and Kozlov (1999)). For Model 1, one packet of six variants is distributed randomly within 23 martensitic blocks, with an average of four blocks per variant as shown in Fig. 3. For Model 2, the same packet of six variants is distributed randomly within 200 martensitic blocks, with an average of 35 blocks per variant as shown in Fig. 3.

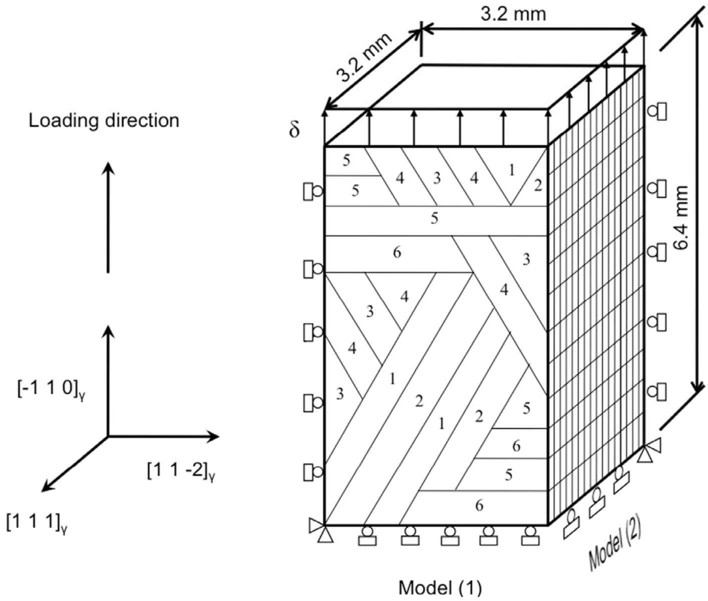

Figure 3: Microstructural model and the distribution of variants in blocks and packets (variants numbered as indicated in Tab. 1).

Using the method outlined by Kameda and Zikry (1996), the initial coefficient values, needed for the evolution of the immobile and mobile densities given by eqs. (6-7) were obtained as

$$g_{minter} = 5.53, \quad g_{recov} = 6.67, \quad g_{immob} = 0.0127, \quad g_{sour} = 2.7 \times 10^{-5},$$

and

$$H/K = 3.289 \times 10^{3\circ}K. \tag{15}$$

Based on a convergence analysis, 2500 (Model 1) and 3000 (Model 2 and 3) four noded quadrilateral elements were used with a plane strain analysis for a specimen size of 3.2 mm by 6.2 mm. The material properties (Tab. 2) that are used here are representative of low nickel alloy steel. The computational framework and the

Table 2: Properties of martensitic grains

Properties	Martensite phase
Young's modulus, E	228 GPa
Static yield stress, τ_y	517 MPa
Poisson's ratio, ν	0.3
Rate sensitivity parameters, m	0.01
Reference strain rate, $\dot{\gamma}_{ref}$	$0.001 s^{-1}$
Critical strain rate, $\dot{\gamma}_{critical}$	$10^4 s^{-1}$
Burger vector, b	3.0×10^{-10}m
Reference stress interaction coefficient, a_i(i=1, 24)	0.5

constitutive formulation used in this study were validated with experimental results, as detailed in the investigation by Hatem and Zikry (2009a).

The global nominal stress-strain curve for Model 1, Model 2, and a multi-packet model is shown in Fig. 4. As seen, the multi-packet model can be projected as an average behavior of both models. These results indicate that the multi-packet model can be potentially obtained by averaging single-packet results for different orientations.

To gain further insight into this behavior, we investigated deformation contours for the different loading planes. As shown in Fig. 5a, the accumulated maximum plastic shear is 2.2 at a nominal strain of 15% for Model (1). This large value is due to dislocation-density activities along different slip-systems, geometrical softening, and the orientation effects associated with the shear pipe effects, which are essentially conduits for localization in martensitic steels as presented by Hatem and Zikry (2009b). The geometrical softening occurs due to the large lattice rotation that as high as 17.9° (Fig. 5b). As can be seen from Fig. 5c, the shear-strain localization is considerably less and discontinuous for Model (2), where the maximum shear slip value is 1.8, combined with high lattice rotation of -33.0 ° (Fig. 5d) as a result of the high angle misorientation relations existing between some blocks.

High and low angle GB relations can be obtained relative to variant sequences. These sequences can be used to determine the compatibility of the slip systems between variants, a summary of these relations is listed for variants 1-6 (V1-V6) in Tab. 3.

For group 1, crystals are based on twin relations; compatible slip-systems are parallel and aligned with the long direction of laths. Group 2 are variants with low angles of approximately 10°. Group 3 relates compatible slips-systems with low angle GBs (with misorientations of less than 10°). Group 4 relates compatible slip-

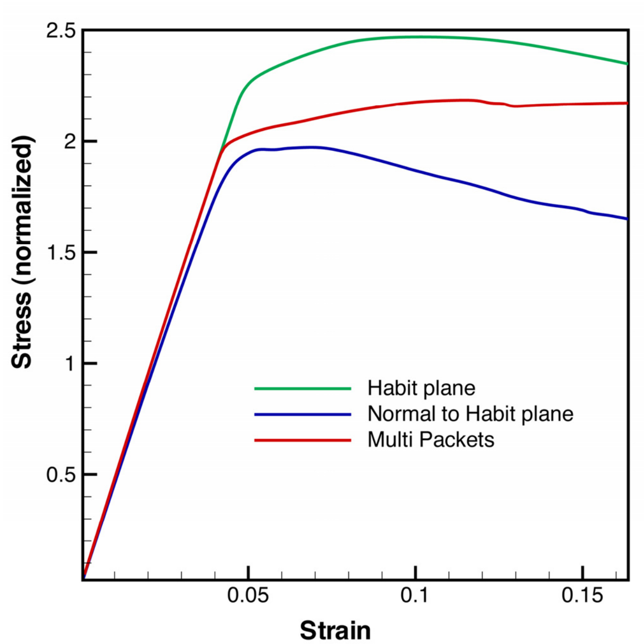

Figure 4: Global stress-strain curve for single packet models (Model 1 and 2), compared with result obtained for multi-packet model of low nickel martensitic steel.

Table 3: The angle between slip systems for variants 1-6 (a packet with habit plane of $(111)_{\gamma}$) that can be divided into groups of high and low angle GB directions.

Group	Variants pair	Angle between
1	V1-V2, V3-V4, V5-V6	0 degree
2	V1-V4, V3-V-6, V2-V5	10.5 degree
3	V1-V3, V1-V5, V2-V4, V2-V6, V3-V5, V4-V6	10.5 degree
4	V1-V6, V2-V3, V4-V5	21 degree

systems with high angle GBs (with misorientations greater than 20°). Furthermore, relations can be obtained for variants belonging to different packets. High angle relations can impede the dislocation-density evolution between certain variant pairs, while low angle relations can promote dislocation-density transmission between other variants, which can lead to shear-strain accumulation and localization (Hatem and Zikry (2009c)).

The current analysis is consistent with experimental results for a single-packet

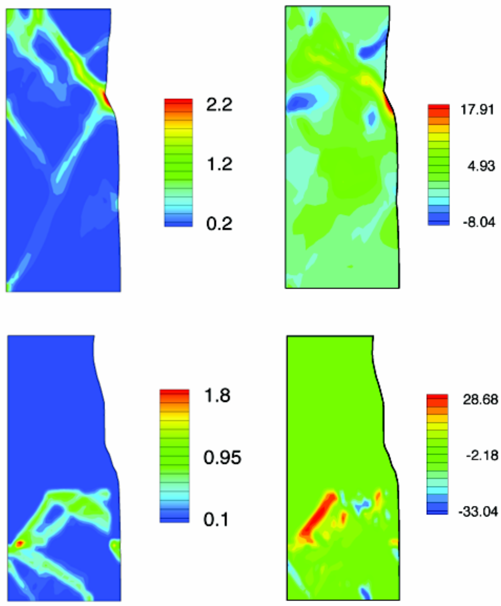

Figure 5: Results obtained from single packet specimens, at nominal strains of 15%. (a) shear slip (b) lattice rotation in degrees, both for Model (1). (c) shear slip (d) lattice rotation in degrees, for Model (2).

martensitic steel microstructure as discussed by Shtremel, Andreev and Kozlov (1999). The strength is higher for the loading plane along the habit plane (Model 1) as compared with those normal to the habit plane model (Model 2) as indicated in Fig. 4. Furthermore, shear-strain localization formation for the habit plane model (Model 1) is consistent with results by Shtremel, Andreev and Kozlov (1999) and the shear pipe effects (Hatem and Zikry (2009)). Localization evolves along the long direction of the laths and parallel to the habit plane. This is due to the slip-systems' orientation relative to the loading axis and the long direction of laths and the low-angle relation between blocks. For the loading plane normal to the habit plane, shear strain localization does not occur. This behavior can explain the highly anisotropic behavior of martensitic steel relative to its block and packet microstructures.

5.1 Fracture Behavior of Single-Packet Lath Martensite

In this section, we investigate interaction scenarios between shear-strain localization regions and cracks that are located in areas of high plastic deformation. We introduce a micro-crack within the shear-strain localization area; the crack length is 0.4 mm. For this analysis, we use the previous variant arrangement and material properties.

The shear slip and the normal stresses normalized by static yield stress are presented in Fig. 6. The maximum shear slip at a nominal strain of 15% is 3.64 (Fig. 6a) combined with maximum normalized normal stress of 4.5 (Fig. 6b) for Model (1). For Model (2), the maximum shear slip at a nominal strain of 15% is 0.8 (Fig. 6c) and the normalized normal stress is 3.6 (Fig. 6d). These results indicate that increases in ductility (or toughness) for Model (1) are due to high dislocation-densities activities ahead of the crack front, which is consistent with analyses by Rice (1992), Kameda and Zikry (1998, 2006), Qiao and Argon (2003), and Hatem and Zikry (2009d).

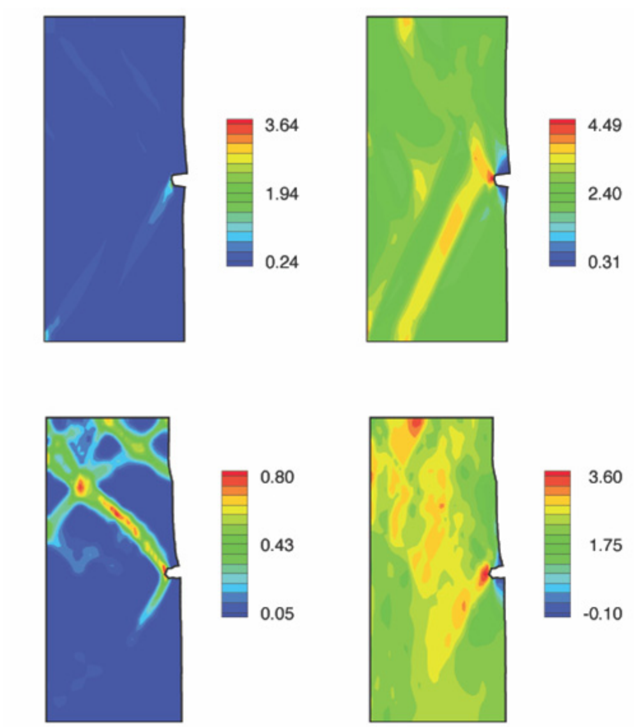

Figure 6: Crack behavior at nominal strains of 15%. (a) shear slip (b) normalized normal stresses, for maraging steel. (c) shear slip (d) normalized normal stresses for ausformed steel.

5.2 Physically Representative Microstructures: SEM/EBSD Steel Microstructures

To further understand the behavior of martensitic steel packets and to be consistent with experimental observations, SEM/EBSD characterized lath martensite for maraging and ausformed steels (18 wt.% Ni steel, see Morito, Kishida and Maki (2003) for more details) were mapped directly into the computational models by extrapolating the geometrical coordinates, and then discretized into a finite-element mesh, as shown in Fig. 7. By ausforming the maraging steel at 773 K, the blocks' width decreased from 18.6 μm to 2.5 μm; initial dislocation-densities increased from $0.91\times10^{15}/\mathrm{m}^2$ to $1.30\times10^{15}/\mathrm{m}^2$, and there were more higher angle misorientation relation between blocks in a single packet, (Morito, Kishida and Maki (2003)). We used these ausformed characteristics and properties in our analysis.

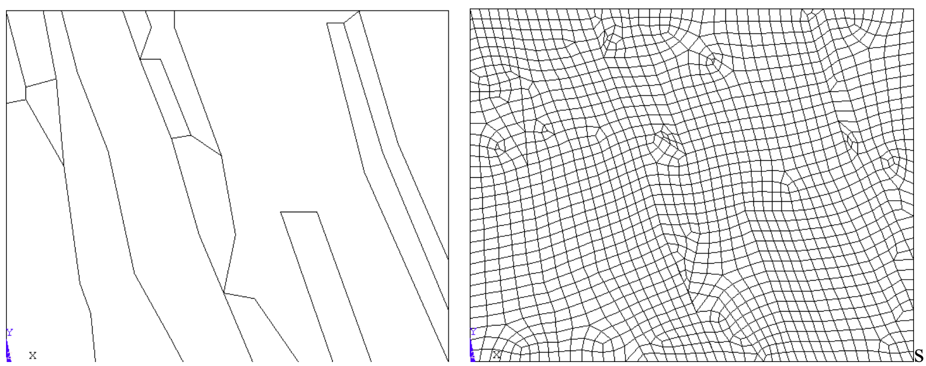

(a) (b)

Figure 7: Physically representative microstructure mapped from SEM/EBSD maraging steel microstructure, Kishida and Maki (2003) in (a), and the finite-element mesh used (b).

Fig. 8 shows the shear slip and normal stresses normalized by static yield stress at nominal strains of 15% for margining steel (a, b) and ausformed steel (c, d). The maximum shear slip is 1.4 at a nominal strain of 15% with a maximum normalized normal stress of 6.1 for the maraging steel. For the ausformed steel, the maximum shear slip is 0.79 and the maximum normalized normal stress is 7.3. Due to the large blocks width and lower number of high-angle relations between blocks in maraging steel, shear-strain localization occurs with lower stresses. In the ausformed steel, there is less accumulation of shear strain with higher stresses, as it would be expected for the ausformed case. These results indicate how physical microstructures can be used with the proposed framework to predict behavior at the relevant martensitic microstructural scale for different martensitic structures.

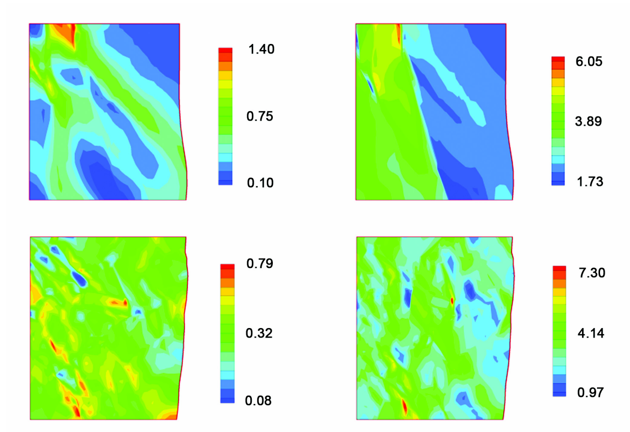

Figure 8: Results obtained from mapped experimental specimens, at nominal strains of 15%. (a) shear slip (b) normalized normal stresses, both for maraging steel. (c) shear slip (d) normalized normal stresses for ausformed steel.

6 Summary

A physically-based microstructural representation of variants, blocks, packets, and initial dislocation-densities for lath martensitic steels was developed. A multiple-slip rate-dependent crystalline constitutive formulation that is coupled to the evolution of mobile and immobile dislocation-densities, and specialized finite-element schemes were used to investigate deformation and failure in a single-packet of lath martensitic steel. Two loading planes have been investigated: along the habit plane and normal to the habit plane.

It has been shown that both the strength and the toughness increase along the habit plane. Shear-strain localization occurs due to shear pipe effects where localization occurs along the long direction of laths and parallel to the habit due to the slip-systems' orientation relative to the load and the long direction of laths and the low-angle relation between blocks. For loading directions normal to the habit plane, there is no shear strain localization, which clearly indicates how the loading plane orientation relative to the habit plane can result in significantly different behavior.

The effects of ausforming process for single-packet microstructures obtained using SEM/EBSD in margining and ausformed steels were also analyzed (Morito, Kishida and Maki (2003)). The ausformed steel had lower propensity for shear strain accumulation.

The present study underscores how the local and unique block and packet microstructures related with the ORs of martensitic steel are intricately linked to deformation, shear-strain localization, and material failure at different physical scales that are unique to martensitic steels.

Acknowledgement: Support from the Office of Naval Research through Grant N000140510097, is gratefully acknowledged.

References

Ashmawi, W. M.; Zikry, M. A. (2000): Effects of Grain Boundaries and Dislocation Density Evolution on Large Strain Deformation Modes in fcc Crystalline Materials. *J. Comput.-Aided Mater. Des.*, vol. 7, pp. 55-62.

Bandstra, J. P.; Koss, D. A.; Geltmacher, A.; Matic, P. ; Everett, R. K. (2006): Modeling void coalescence during ductile fracture of a steel. *Mater. Sci. Eng A-Struct.*, vol. 366, no. 2, pp. 269-281.

Bay, B.; Hansen, N.; Hughes, D. A.; Kuhlmann-Wilsdorf, D. (1992): Evolution of F.C.C. Deformation Structures in Polyslip. *Acta Metall. Mater.*, vol. 40, pp. 205-219.

Bhadeshia, H. K. D. H. (2001): *Worked examples in the geometry of crystals.* The institute of metals, London.

Franciosi, P. (1983): Glide mechanisms in b.c.c. crystals: an investigation of the case of Alfa Iron through multislip and latent hardening test. *Acta Metall.*, vol. 31, no. 9, pp. 1331-1342.

Grujicic, M.; Dang, P. (1995): Computer simulation of martensitic simulation of martensitic transformation in Fe-Ni face-centered cubic alloys. *Mater. Sci. Eng A-Struct.*, vol. 201, pp. 194-204.

Hansen, N. (1990): Cold Deformation Microstructures. *Mater. Sci. Technol.*, vol. 6, pp. 1039-1047.

Hatem, T. M.; Zikry, M. A. (2009a): Dislocation-Density Crystalline Plasticity Modelling of Lath Martensitic Microstructures in Steel Alloys. *Philos. Mag.*, vol. 89, no. 33, pp. 3087-3109.

Hatem, T. M.; Zikry, M. A. (2009b): Shear Pipes Effect and Shear-Strain Localization in Martensitic Steels. *Acta Mat.*, vol. 57, no. 15, pp. 4558-4567.

Hatem, T. M.; Zikry, M. A. (2009c): Modeling of Lath Martensitic Microstructure and Failure Evolution in Steel Alloys. *J. Eng. Mater-T ASME*, vol. 131, no.

041207, pp. 1-10.

Kameda, T.; Zikry, M. A. (1996): Three Dimensional Dislocation-Based Crystalline Constitutive Formulation for ordered Intermetallics. *Scripta Mater.*, vol. 38, no. 4, pp. 631-636.

Kameda, T.; Zikry, M. A. (1998): Intergranular and transgranular crack growth at triple junction boundaries in ordered intermetallics. *Int. J. Plast.*, vol. 14, no.8, pp. 689-702.

Kameda, T.; Zikry, M. A.; Rajendran, A. M. (2006): Modeling of grain-boundary effects and intergranular and transgranular failure in polycrystalline intermetallics, *Metall. Mater. Trans. A*, vol. 37A, pp. 2107-2115.

Kelly, P. M. (1992): Crystallography of Lath Martensite in Steels. *Mater. Trans. JIM*, vol. 33, no. 3, pp. 235-242.

Krauss, G. (2001): Deformation and Fracture in Martensitic Carbon Steels Tempered at Low Temperature. *Metall. Mater. Trans. A*, vol. 32B, pp. 205-221.

Liu, Q.; Jensen, D. J.; Hansen, N. (1998): Effect of Grain Orientation on Deformation Structure in Cold-Rolled Polycrystalline Aluminium. *Acta Mater.*, vol. 46, no. 16, pp. 5819-5838.

Marian, J.; Wirth, B. D.; Schaublin, R.; Odette, G. R.; Perlado, J. M. (2003): MD modeling of defects in Fe and their interactions. *J. Nucl. Mater.*, vol. 323, pp. 181-191.

McVeigh, C.; Vernerey, F.; Liu, W. K.; Moran, B.; Olson, G. B. (2007): An interactive micro-void shear localization mechanism in high strength steels. *J. Mech. Phys. Solids*, vol. 55, pp. 225-244.

Morito, S.; Tanaka, H.; Konishi, R.; Furuhara, T.; Maki T. (2003a): The Morphology and Crystallography of Lath Martensite in Fe-C Alloys. *Acta Mater.*, vol. 51, pp. 1789-1799.

Morito, S.; Kishida, I.; Maki, T. (2003b): Microstructure of Ausformed Lath Martensite in 18%Ni Maraging Steel. *J. Phys. IV France*, vol. 112, pp. 453-456.

Morito, S.; Nishikawa, J.; Maki, T. (2003c): Dislocation Density within Lath Martensite in Fe-C and Fe-Ni Alloys. *ISIJ Int.*, vol. 43, no. 9, pp. 1475-1477.

Morito, S.; Saito, H.; Ogawa, T.; Furuhara, T.; Maki T. (2005): Effect of Austenite Grain Size on the Morphology and Crystallography of Lath Martensite in Low Carbon Steels. *ISIJ Int.*, vol. 45, no. 1, pp. 91-94.

Morito, S.; Yoshida, H.; Maki, T.; Huang, X. (2006a): Effect of Block Size on the Strength of Lath Martensite in Low Carbon Steels. *Mater. Sci. Eng A-Struct.*, vols. 438-440, pp. 237-240.

Morito, S.; Huang, X.; Konishi, R.; Furuhara, T.; Maki T. (2006b): The Morphology and Crystallography of Lath Martensite in Alloys Steels. *Acta Mater.*, vol. 54, pp. 5323-5331.

Mughrabi, H. (1987): A 2-Parameter Description of Heterogeneous Dislocation Distributions in Deformed Metal Crystals. *Mater. Sci. Eng.*, vol. 85(1-2), pp. 15-31.

Nakagawa, H.; Miyazaki, T. (1999): Effect of Retained Austenite on the Microstructure and Mechanical Properties of Martensitic Precipitation Hardening in Stainless Steel. *J. Mater. Sci.*, vol. 34, pp. 3901-3908.

Qiao, Y.; Argon, A. S. (2003): Cleavage cracking resistance of high angle grain boundaries in Fe–3%Si alloy. *Mech. Mater.*, vol. 35, pp. 313-331.

Rice, J. R. (1992): Dislocation nucleation from a crack tip: An analysis based on the Peierls concept. *J. Mech. Phys. Solids*, vol. 40, no. 2, pp. 239-271.

Rowenhorst, D. J.; Gupta, A.; Feng, C. R.; Spanos, G. (2006): 3D Crystallography and Morphological Analysis of Coarse Martensite: Combining EBSD and Serial Sectioning. *Scripta Mater.*, vol. 55, pp. 11-16.

Sandvik, B. P. J.; Wayman, C. M. (1983): Characteristics of Lath Martensite, I, II, III. *Metall. Trans. A*, vol. 14A, pp. 809-822, 823-834, 835-844.

Shtremel, M.A.; reev, Yu. G.; Kozlov. D. A. (1999): Structure and Strength of Lath Martensite. *Metall. Sci. Heat Treatment*, vol. 41, pp.140-145.

Stainier, L.; Cuitino, A. M.; Ortiz, M. (2002): A micromechanical model of hardening, rate sensitivity and thermal softening in b.c.c single crystal. *J. Mech. Phys. Solids*, vol. 50, pp. 1511-1545.

Suzuki, T.; Shimono, M.; Ren, X.; Otsuka, K.; Onoder, H. (2006): Study of martensitic transformation by use of Monte-Carlo method and molecular dynamics. *Mater. Sci. Eng A-Struct.*, vols. 438-440, pp. 95-98.

Wasaka, W.; Wayman, C. M. (1981a): The Morphology and Crystallography of Ferrous Lath Martensite. Studies of Fe-20%Ni-5%Mn-I, II, III. *Acta Metall.*, vol. 29, pp. 973-990, 991-1011, 1013-1028.

Wasaka, W.; Wayman, C. M. (1981b): Crystallography and Morphology of Ferrous Lath Martensite. *Metallography*, vol. 14, pp. 49-60.

Zhai, J.; Tomar, V.; Zhu, M. (2004): Micromechanical simulation of dynamic fracture using cohesive finite element method. *J. Eng. Mater-T ASME*, vol. 126, pp. 179-191.

Zikry, M. A. (1994): An Accurate and Stable Algorithm for High Strain-Rate Finite Strain Plasticity. *Comput. Struct.*, vol. 50, pp. 337-350.

Zikry, M. A.; Kao, M. (1996): Inelastic Microstructural Failure Mechanisms in Crystalline Materials with High Angle Grain Boundaries. *J. Mech. Phys. Solids*, vol. 44, no. 11, pp. 1765-1798.